Ethanol Electrooxidation at Platinum-Rare Earth (RE = Ce, Sm, Ho, Dy) Binary Alloys

D.M.F. Santos [1,*] , **J.R.B. Lourenço** [1], **D. Macciò** [2], **A. Saccone** [2], **C.A.C. Sequeira** [1] **and J.L. Figueiredo** [3]

1   CeFEMA, Instituto Superior Técnico, Universidade de Lisboa, 1049-001 Lisbon, Portugal; joanarblourenco@gmail.com (J.R.B.L.); cesarsequeira@tecnico.ulisboa.pt (C.A.C.S.)
2   Dipartimento di Chímica e Chímica Industriale, Universitá di Genova, I-16146 Genova, Italy; Daniele.Maccio@unige.it (D.M.); adriana.saccone@unige.it (A.S.)
3   Laboratory of Catalysis and Materials, LSRE-LCM, Faculdade de Engenharia, Universidade do Porto, 4200-465 Porto, Portugal; jlfig@fe.up.pt
*   Correspondence: diogosantos@tecnico.ulisboa.pt

Abstract: Proton exchange membrane fuel cells and direct alcohol fuel cells have been extensively studied over the last three decades or so. They have emerged as potential systems to power portable applications, providing clean energy, and offering good commercial viability. Ethanol is considered one of the most interesting fuels in this field. Herein, platinum-rare earth (Pt-RE) binary alloys (RE = Ce, Sm, Ho, Dy, nominal composition 50 at.% Pt) were produced and studied as anodes for ethanol oxidation reaction (EOR) in alkaline medium. A Pt-Dy alloy with nominal composition 40 at.% Pt was also tested. Their electrocatalytic performance was evaluated by voltammetric and chronoamperometric measurements in 2 M NaOH solution with different ethanol concentrations (0.2–0.8 M) in the 25–45 °C temperature range. Several EOR kinetic parameters were determined for the Pt-RE alloys, namely the charge transfer and diffusion coefficients, and the number of exchanged electrons. Charge transfer coefficients ranging from 0.60 to 0.69 and n values as high as 0.7 were obtained for the $Pt_{0.5}Sm_{0.5}$ electrode. The EOR reaction order at the Pt-RE alloys was found to vary between 0.4 and 0.9. The Pt-RE electrodes displayed superior performance for EOR than bare Pt, with $Pt_{0.5}Sm_{0.5}$ exhibiting the highest electrocatalytic activity. The improved electrocatalytic activity in all of the evaluated Pt-RE binary alloys suggests a strategy for the solution of the existing anode issues due to the structure-sensitive EOR.

Keywords: ethanol electrooxidation; Pt-RE alloys; direct ethanol fuel cell; electrocatalysis

1. Introduction

Rising demands for energy, coupled with concerns over environmental pollution and growing fossil fuel costs, have contributed to a great need for clean and efficient power sources [1–4]. To achieve the goal of reducing more than 50% of CO_2 emissions by the year 2050, compared to CO_2 emissions in 2009, as proposed by the International Energy Agency (IEA), the transportation sector must reduce CO_2 emissions dramatically. It is very clear that simply improving the efficiency of internal combustion engines that are subject to Carnot cycle limitations will not be able to achieve such a goal [5,6]. Thus, another high-efficiency conversion device is required as an alternative to the internal combustion engine, or another fuel as an alternative to gasoline is required to reduce CO_2 emissions [1,7,8].

Electrochemical oxidation of small organic molecules is regarded as the most promising technology due to its high thermodynamic efficiency (up to 97%) via low-temperature direct fuel cell reaction [9–12]. Compared with hydrogen, i.e., the fuel used in proton exchange membrane fuel cells (PEMFCs),

room-temperature liquid alcohols, such as ethanol and methanol, are more promising in fuel cell devices for their high volumetric energy densities, better safety, and low-cost generation and storage. While many exciting studies have been reported, there is much to be done to further understand the reactivity, selectivity, and durability of the electrocatalytic processes in the ethanol and methanol oxidation reactions (EOR/MOR) in fuel cells (FCs) [13,14]. As a new energy technology, fuel cells, which are electrochemical power generation devices converting the chemical energy of fuel into electrical energy by an electrochemical reaction, are rapidly developing, and their performance is continually improving. They have the advantages of high-energy-density, clean and environmental protection, self-generation, and high efficiency without Carnot cycle limitation [3,10,13]. The fuel cell stack composed of multiple single-cells is gradually being used in portable electronic products. Direct methanol fuel cells (DMFCs) use methanol (CH_3OH) as a reactant, which has the advantages of being an abundant fuel source, low price, convenient operation, and easy miniaturization. It is suitable as a power source for portable devices [14–16], and it has been considered the most appropriate fuel cell among the direct alcohol fuel cells (DAFCs) [17–19] since methanol is more easily oxidized than other alcohols due to the absence of C-C bonds. However, methanol is a toxic product with sluggish kinetics at the anode, its main limitation being its crossover from the anode to the cathode compartments of the FC, which reduces the cell potential and leads to the formation of undesirable products [17–20]. Further studies have found that temperature affects the quality and momentum transfer of DMFC, methanol concentration, percolation current density, polarization curve, and CO_2 distribution [21,22].
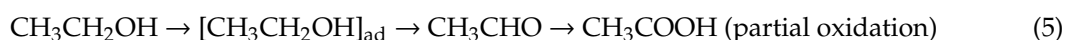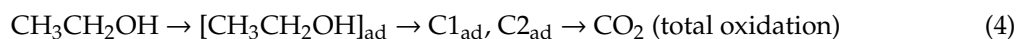
Thus, ethanol (C_2H_5OH) has emerged as an excellent alternative to methanol since it is also a hydrogen-rich liquid fuel but with lower toxicity and higher specific energy (8.0 kWh kg^{-1}) than methanol (6.1 kWh kg^{-1}) [23]. Moreover, ethanol can be produced from renewable sources, such as by fermentation from biomass, which makes it an attractive fuel from both an economic and environmental perspective. The major drawback of using ethanol as a fuel is the necessary C–C bond cleavage to oxidize ln ν plots (Figure 5a) completely and by ethanol to carbon dioxide (CO_2). This reaction withdraws 12 electrons per molecule of ethanol, as shown in Equation (1) [18], which makes this a slow process compared to the electrochemical oxidation of hydrogen and methanol, involving 2 and 6 electrons, respectively [23,24].

$$CH_3CH_2OH + 12\,OH^- \rightarrow 2\,CO_2 + 9\,H_2O + 12\,e^- \tag{1}$$

This oxidation reaction going on at the anode of the DEFC (EOR) is accompanied by an oxygen reduction reaction, as shown in Equation (2), at the cathode of the DEFC (ORR), giving an overall reaction expressed by Equation (3).

$$3\,O_2 + 6\,H_2O + 12\,e^- \rightarrow 12\,OH^- \tag{2}$$

$$CH_3CH_2OH + 3\,O_2 \rightarrow 3\,H_2O + 2\,CO_2 \tag{3}$$
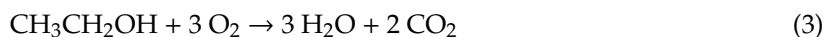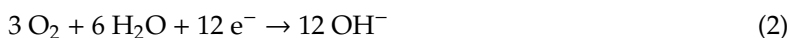
A comprehensive description of the mechanism of EOR is still under investigation by the scientific community, but some general steps are largely accepted. An initial step may involve dehydrogenation, while subsequent steps may lead to intermediates such as acetaldehyde (CH_3CHO) and acetic acid (CH_3COOH) [25,26]. A large number of other intermediates are formed due to the numerous C-H, C-O, and C-C bond scissions that occur during ethanol oxidation. The scientific community has not been able to determine the precise mechanism but only that two general class of adsorbed intermediates, $C1_{ad}$ and $C2_{ad}$, which represent fragments with one and two carbon atoms respectively, are formed, as shown in Equations (4) and (5).

$$CH_3CH_2OH \rightarrow [CH_3CH_2OH]_{ad} \rightarrow C1_{ad}, C2_{ad} \rightarrow CO_2 \text{ (total oxidation)} \tag{4}$$

$$CH_3CH_2OH \rightarrow [CH_3CH_2OH]_{ad} \rightarrow CH_3CHO \rightarrow CH_3COOH \text{ (partial oxidation)} \tag{5}$$

A simple bond analysis between the intermediate and the final product, CO_2, shows that breaking a C-C bond is inevitable. This is one of the most important steps in ethanol electrocatalysis. The difficulty of breaking the C-C bond results in a high concentration of partial oxidation products, CH_3CHO and CH_3COOH, at the surface of platinum (Pt) catalysts, which causes a significant drop in the efficiency of the DEFC. It also substantially alters the environmental aspects of such a device by producing undesirable byproducts, as reported above for DMFCs.
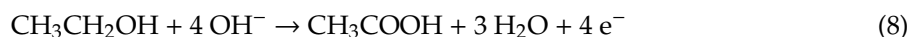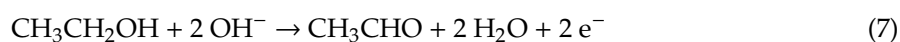
The difficulties to precisely establish the mechanism of the ethanol oxidation reaction (EOR) have led the scientist community to try different ways to understand this reaction. One common approach is to try to improve the reaction associated with the rate-determining step (RDS). For the ethanol decomposition reaction, and more precisely for the C-C bond breaking reaction, the RDS over transition metal has been suggested by different DFT studies [27–31] to be the following step expressed in Equation (6).

$$CHCO_{ads} \rightarrow CH_{ads} + CO_{ads} \tag{6}$$

It should be noted that these results were obtained considering the ethanol decomposition and not the ethanol oxidation (the reaction occurring in a fuel cell), but this approach was recently shown to give results in agreement with the experiment to compare pure Pt to pure iridium and Ir/Ru alloy [32,33]. Experimental studies also proposed the same intermediates for the C-C bond breaking reaction at the surface of a Pt or iridium catalyst [26,34–36].

Catalysis is a surface effect, so the size of the surface has a crucial importance on the performance of the catalyst since the more extensive the surface, the more adsorption sites are available for the reactants. Consequently, since only the surface (and the few layers underneath are of importance) a typical type of catalyst is made by dispersing the active phase on conductive support like carbon, to avoid excessive use of catalyst material and, thus, saving money. Although carbon-supported Pt is one of the most used anode catalysts in low-temperature fuel cells, it is far from being the most efficient one for the DEFC.

To improve the catalyst efficiency for the EOR, and also for the ORR, it is necessary to find new electrocatalysts that would increase the overall kinetics of the reactions, but also to shift the EOR towards complete oxidation. This would release more electrons, and thus more energy at the outlet of the fuel cell. In other words, it increases the selectivity of the reaction towards CO_2 formation [37]. Indeed, on the current Pt-based anode catalyst, the incomplete oxidation of ethanol produces acetaldehyde (Equation (7)) and acetic acid (Equation (8)), which delivers only 2 and 4 electrons [25,26]. This incomplete oxidation process needs to be compared to the complete oxidation that forms CO_2 and releases a set of 12 electrons [25,26].

$$CH_3CH_2OH + 2\,OH^- \rightarrow CH_3CHO + 2\,H_2O + 2\,e^- \tag{7}$$

$$CH_3CH_2OH + 4\,OH^- \rightarrow CH_3COOH + 3\,H_2O + 4\,e^- \tag{8}$$

DEFC anode catalysts have been extensively studied, but most of the work has been performed using Pt [38–42]. Nevertheless, it has been shown that the loading of Pt needs to be reduced by a factor of 3 to achieve an economically viable device [43]. Different methods have been employed to do so, such as reducing the Pt loading by using alloys instead or a pure Pt catalyst, by using carbon supports, or even using other materials like carbides and oxides as an anode catalyst [44].

One major challenge encountered by the current ethanol fuel cell catalyst based on Pt is its strong tendency to be poisoned by CO [45,46], which is an intermediate in the oxidation reaction or can be present in fuel streams. Pt binds too strongly with the molecule, leading to a catalyst surface almost saturated with carbon monoxide [36]; this results in not having enough free surface area for the oxygen to adsorb and, consequently, to oxidize CO into CO_2 [36,47].

This poisoning effect needs to be overcome by modifying the surface so that the oxygen coverage can be increased via the adsorption of OH coming from the dissociation of water. The modification of the surface is often done by adding another element [37,47–51] that changes the properties or by

even adding a third one in some cases [48]. Other methodologies include the control of the catalyst morphology and choosing appropriate support materials [52–54]. The incorporation of a second metal into Pt can provide oxygen-containing species at lower potentials and reduce the bond strength of Pt-CO$_{ads}$ and then support the oxidation removal of CO to CO_2 [53], helping the development of liquid fuel oxidation kinetics considerably [52,55–57]. Different alloy structures have been studied, from doping to near-surface alloys (NSA) [58], or even core/shell structures [46,59]. NSA's regroup the catalysts that are made of an atomic layer of a transition metal inserted in the top or second layer of a catalyst, while a core/shell structure is a structure where strong segregation between the metals constituting the alloy exists, and where one of them tends to segregate towards the surface (the shell) and the other preferentially stays inside (the core). Finally, doping is a technique that consists of introducing a few atoms in the structure of a catalyst to slightly modify its electronic properties. Two of the most efficient catalysts involving Pt deserve some considerations, as discussed below.

Concerning the oxidation mechanism of ethanol, Schmidt et al. [60] observed that the presence of ruthenium partially inhibits the formation of chemisorbed species coming from dissolved ethanol. Hence, in oxidation happening mostly with weakly adsorbed species, the selectivity between partial and complete oxidation of ethanol was found to be higher compared to pure Pt. Indeed, the authors claim that ruthenium addition enhanced ethanol oxidation performance, probably due to the strong adsorption of OH on the Ru sites. Tests in direct ethanol fuel cells showed that the cells with Pt-Ru/C as anode material perform better than those with Pt/C [60–63]. Pt-Ru/C always demonstrated a maximum power density (MPD) for a single DEFC in the range 70–100 °C superior to the one with Pt/C as anode catalyst.

The other efficient binary catalyst is typically composed of an fcc Pt-Sn alloy and Sn and Pt oxides. The relative amount of Pt-Sn alloy versus SnO_2 affects strongly the electrochemical activity of these catalysts. DEFCs with Pt-Sn/C as anode material performed better than those with Pt-Ru/C [60,61,64,65].

The performance of various Pt-Sn/C (2:1) and Pt-Ru/C (1:1) catalysts as anode materials were compared by Song et al. [66], and they showed that the preparation method has a significant effect. They prepared a binary catalyst Pt-Sn/C in two different ways and obtained different results depending on the current density. Pt-Sn/C with different preparation methods shows almost similar behavior for low current density, however, increasing the current density results in a variation of the performance of the cell. This difference is attributed, according to the authors, to the higher content of Sn oxide one of the two preparations, leading to a higher internal cell resistance, which consequently affects the cell performance.

The advantage of alloy structures is no longer required to be proven, with numerous binary structure already tested; for example, Pt-M, with M = W, Pd, Rh, Re, Mo, Ti, Ce, Mn, Ni, and Cu always demonstrating a higher EOR activity than pure Pt as an anode catalyst [48,67–74].

The incorporation of Rh and SnO_2 into Pt has been recognized to considerably enhance the liquid fuel oxidation kinetics. SnO_2 provides OH species to oxidize adsorbed residues and enhances the formation of acetaldehyde and acetic acid. On the other hand, the addition of Rh further increases the EOR activity and stability by promoting the C-C bond cleavage, thus improving the electrocatalytic performance in DEFCs [29,75–77]. In this context, Adzic's group showed by in situ infrared reflection-absorption spectroscopy (IRRAS) that the integrated band intensities of CO_2 (2343 cm^{-1}), CH_3CHO (933 cm^{-1}), and CH_3COOH (1280 cm^{-1}) for both Pt-Rh-SnO$_2$/C and Pt-SnO$_2$/C samples proved the enhanced cleavage of the C-C bond in ethanol and all three constituents Pt, Rh, and SnO_2 are needed to gain the synergistic effect in facilitating the total oxidation of ethanol [78]. Their promising family of EOR nanocatalysts based on mixtures of Pt, Rh, and Sn has been studied in alkaline and acid media, showing the highest activity for a composition of Pt:Rh:Sn = 3:1:4 [78,79] for EOR in acidic solutions.

It should be noted at this point, that apart from Adzic's group, many other workers are currently reporting EOR studies in both alkaline and acidic solutions, which seems acceptable because, in both media, the same reaction mechanism applies [80–82]. However, the increase in pH will change the

reaction product distribution. With spectroscopic experiments, it has been found that on a Pt surface, the main ethanol oxidation product is acetate [83] (acetic acid in alkaline medium dissociates rapidly to acetate ion, CH_3COO^-). Moreover, the C-C cleavage most probably occurs via an acetaldehyde molecule where the α-hydrogen atom (in the CH_3 group) is slightly acidic, causing deprotonation of acetaldehyde in high pH electrolytes. When the charge is delocalized at the one end of the molecule, the C-C bond becomes less shielded and is easier to break. Combining more facile C-C bond cleavage and the fact that CH_x [84] and CO_{ads} [85,86] can be adsorbed at the lower potential in an alkaline medium, it could be deduced that selectivity towards a C-C bond rupture pathway is enhanced.

The use of the computation-guided method and the discovered structure-property relationship established a rational strategy to aid the development of EOR catalysts for possible commercialization of DEFCs. Accordingly, Abruña et al. [87] investigated the promotion roles of additive metals in ternary Pt-Sn-M (M = Fe, Ni, Pd, Ru) catalysts toward EOR, via a combination of theoretical calculations and experimental evidence. They found that the variation and combination of different compounds could exert better electrocatalytic performance with different electronic effects. Their Fe-containing catalysts exhibited the highest activity, followed by Ni- and Pd-containing materials with similar results. Bimetallic or ternary nanocrystals (NCs) have also been studied to explore the optimum combination of higher activity surface facets and electronic effects. In this context, a powerful conceptual approach to design, synthesize, and optimize single-crystalline Pt-Pd-Rh NCs of altered shapes and compositions based on combined density functional theory (DFT) calculations and experimental study was reported by Zhu et al. [88]. They prepared (111)-terminated Pt-Pd-Rh nanotruncated-octahedrons (NTOs) and (100)-terminated Pt-Pd-Rh nanocubes (NCus) with varied compositions, by regulating the reduction tendency of metal precursors in a facile hydrothermal method. Among their catalysts, PtPdRh NTOs exhibited the highest selectivity to carbon dioxide, and PtPdRh NCus possessed the best durability. Combined with in situ FTIR and by adjusting the surface composition and morphology of PtPdRh NCs, it was found that (100)-bounded surface is favorable to the cleavage of the C-C bond, while (111)-bounded surface tends to oxidize CO more easily. As discussed above, Pt and alloys of Pt with 3d metals have been optimized to producing promising new groups of catalysts. However, further work into phase purity and alloying conditions are needed to fully realize their potential. In fact, in accelerated testing these alloys can also exhibit great stability if the catalyst is annealed before testing, however, long term stability is still uncertain [89,90]. Under reaction conditions, the driving force for the dissolution of the solute metal is substantial, and the factors that will determine long-term stability are thermodynamic stability of the alloy and kinetic barriers for intermediate diffusion [91,92].

In 2009, Greeley et al. published an article describing a new class of alloys that were screened using the thermodynamic stability as a parameter together with the weakening of the *O binding energy [93]. When performing the theoretical work, Pt_3Y was identified as a suiting candidate, exhibiting high alloying energy and a weakened *O binding energy. The subsequent electrochemical measurements of the polycrystalline sample revealed a six-fold activity enhancement for ORR compared to pure Pt.

Since the initial publication, many other groups around the world have continued to work with this design philosophy of thermodynamic stability. With this work, they have brought new insight into the activity, structure, and stability of the Pt_3Y alloy and subsequent alloys containing lanthanide and alkali earth metals [94–97]. Malacrida et al. [98] expanded the group of alloys studied by Greeley [93], including many of the lanthanide metals and even alkali earth metals [94–98]. The enthalpy of formation for the examined platinum-rare earth (Pt-RE) alloys are significantly more negative than that for the well-known 3d metal alloys [99–103]. Under the assumption that thermodynamic stability plays a role for long-term stability, these Pt_xM alloys, where M = Y, La, Ce, Gd, and x = 3 or 5, exhibit the right trend in alloying energy.

A theoretical study from 2015 by Vej-Hansen et al. [92] into diffusion barriers of alloys revealed an overall correlation between alloying energy and barriers for bulk diffusion of solute metal. For alloys of M_3X with M = Pt, Pd, Al, and X = Fe, Co, Cu, Ni, the barriers for interatomic diffusion increased with the alloying energy. While these calculations were carried out on alloys with the cubic Cu_3Au

structure, the authors argue that this correlation should also hold for other structures, however, the dependence may change [92]. As a result, the substantial enthalpy of formation for the Pt-RE alloys provides them with kinetic stability through barriers for bulk diffusion. However, the standard potential for dissolution of the various rare earth (RE) metals fall below −2.3 V, meaning that the overall thermodynamic driving force for dissolution is ≈−10 eV at a potential of 1 V. When factoring in the stabilization offered by alloying of ≈4 eV, the thermodynamic driving force for dissolution becomes ≈−6 eV. The thermodynamic driving force for dissolution of the RE is therefore strong even when factoring in the strong heat of formation for these alloys.

The initial modeling of the active Pt_3Y assumed a single monolayer of pure Pt on top, the Pt-skin surface that was observed for the Pt_3Ni system. In doing so, the ligand effect was the main contributor to the weakening of the *O binding energy [93]. For later publications by Stephens et al. [94,95] and Escudero-Escribano et al. [96] used angle-resolved X-ray photoelectron spectroscopy (AR-XPS) to probe the elemental composition of the alloys before and after electrochemical measurements [94–96]. After electrochemical measurements, an overlayer of Pt had formed of two to four monolayers (MLs) in thickness. The third overlayer of pure Pt excludes the ligand effect from having any influence on the activity and leaves only strain effects to alter the binding energies [94–104]. At the same time, over the accelerated stability measurement, these alloys retain most of their activity. While Pt_5Tb has the highest initial activity, Pt_5Gd retains the most activity and is still five times as active as Pt after stability measurements. From the work by Escudero-Escribano et al. [97] it is possible to order the alloys by initial specific activity at 0.9 V vs. RHE of Pt and show that for the Pt_5M alloys their highest activity begins with Pt_5Tb and decreases as one goes to the right, with pure Pt at the end: Tb, Gd, Sm, Dy, Tm, Ce, La, and Pt. In addition, the ORR activity of Pt_5Ca is similar to that of Pt_5Dy. Studies by Stephens et al. [94], Escudero-Escribano et al. [97], and Strasser et al. [105] reveal that by comparing the bulk lattice parameters of the Pt_5-RE alloys to that of pure Pt, it can be observed that the strain would range from 3% to 6%, more than predicted for optimal *OH binding energy. In the real system, approaching the high levels of strain in these structures would cause dislocations in the Pt overlayers and relaxation, lowering the overall strain on the surface [105]. This relaxation can explain the decrease in activity observed as the alloys go beyond Tb in the lanthanide series. The actual stability of these alloys can be questioned, with the observation that the higher the initial activity, the higher the leaching of the alloying metal. Erlebacher et al. [106] argue that for core-shell nanoparticles, surface diffusion of Pt is sufficient for creating pinholes in the surface, allowing the dissolution of the alloying metal in the core. Coupled with this, Shao-Horn et al. [107] have shown that the decreased dissolution potential observed for alloys with increased alloying energy causes excessive and continued leaching of the metal for similar-sized particles. With this, the Pt-RE alloys and their proposed stability seem less likely. However, the intermediate structure of the Pt-RE alloys and the increased kinetic barriers predicted for these could still prove indispensable for real long-term stability. To further understand the activity and stability of the Pt-RE catalysts, more studies are required, namely for these alloys in nanoparticulate form, as are beginning to appear more recently [108–110]. Still in this context, the electronic interactions and the microstrain effects on the enhancement of the catalytic activity of Pt for ethanol electrooxidation through synergetic interactions was very recently reported by Paulo et al. [111], using Pt nanoparticles modified with small amounts (≤5 wt.%) of CeO_2 in acid medium. By investigating this system, the authors put in evidence the oxygen donor capability of CeO_2 and the importance of Ce^{4+} ions in the reaction, as shown in Equation (9), attributing the electronic effects to the CeO_2 semiconductor substrate, and the important strain of the Pt lattice during particle growth (that could change the surface free energy of the system) to the presence of very small amounts of CeO_2. Further investigation of Pt-CeO_2 materials has also been published recently [112–114].

$$Pt\text{-}CO_{ads} + 4\,CeO_2 + H_2O + 2\,e^- \rightarrow 2\,Ce_2O_3 + Pt + CO_2 + 2\,OH^- \tag{9}$$

Novel approaches for the synthesis of noble metal-based RE nanoalloys are considered promising for the preparation of electrocatalytic materials for fuel cell applications. For example, Xiang et al. [115]

developed a controllable synthesis route in deep eutectic solvents of concave cubic Pt-La alloy nanocrystals with the average size of 47.5 nm and uniform distributions, as well as adjacent high-index facets, and this open structure can provide an abundance of surface active sites such as the high charge density atomic steps and kinks. Combined with the high charge-transfer interactions between Pt and La, the synthesized material exhibits enhanced specific current density and long-term durability for the EOR.

Apart from Ce and La, other REs (e.g., Eu, Nd, Pr) have been added to Pt and Pt-based alloys, and their effect on the ethanol oxidation efficiency and mechanism has been investigated [116–119]. Despite the progress reported above for the rational design of high-performance EOR catalysts, several fundamental and practical issues of catalysts remain to be addressed [120–123]. In the case of Pt-RE materials, advances have significantly propelled the development of the cathodes of DEFCs and other FCs, but high-performance Pt-RE anodes remain in its infancy. In this domain, the authors have developed efficient Pt-RE anodes and cathodes for direct borohydride fuel cells [124–126] and the hydrogen evolution reaction in alkaline electrolyzers [127,128]. At present, they are also studying the electrocatalysis of oxygen reduction at Pt-RE alloys for application in PEMFCs.

In this work, Pt-RE binary alloys, the RE elements being cerium (Ce), samarium (Sm), dysprosium (Dy), and holmium (Ho) were produced by induction heating and analyzed by SEM/EDS and XPS. Their electrocatalytic activity for EOR in alkaline media was evaluated using cyclic and linear scan voltammetry and chronoamperometry in the 25–45 °C temperature range. The ethanol diffusion coefficient and several kinetic parameters were determined, including the number of exchanged electrons, transfer coefficients, and the reaction order. The present results and conclusions are expected to provide vital kinetic data for the Pt-RE/ethanol system and to have substantial implications for new and efficient ethanol-based fuel cells.

2. Experimental

2.1. Preparation of the Pt-RE Electrodes

Pt-RE binary alloys were prepared as buttons by mixing stoichiometric amounts of Pt and RE elements, namely Ce, Sm, Dy, and Ho, in tantalum crucibles, and then melted by induction heating under Argon flow, following the previously reported procedure [128]. The synthesis in the sealed crucible was particularly useful in the case of Sm to avoid its evaporation due to the high vapor pressure. To ensure the buttons homogeneity, all samples were remelted up to four times. Four of the Pt-RE alloy samples, with RE = Ce, Sm, Dy, and Ho, had a nominal composition of 50 at.% Pt, with one additional PtDy alloy sample having 40 at.% Pt. To produce the electrodes, the alloy buttons were glued with silver glue to copper cables, placed in Epoxy resins, and then polished until obtaining smooth surfaces.

2.2. Catalysts Characterization

Scanning electron microscopy (SEM, Carl Zeiss SMT Ltd., Cambridge, UK) coupled with energy dispersive X-ray analysis (EDS) was used to characterize the morphology of the five tested Pt-RE alloys and to confirm their phase composition. SiC papers and diamond pastes with grain size down to 1 mm were used to smooth the alloys' surfaces and prepare them for microscopic observation. An acceleration voltage of 20 kV was applied for the quantitative analysis, with calibration being done with a Co standard. The Inca Energy software package (Oxford Instruments, Abingdon, UK) was used to process the X-ray spectra.

X-ray photoelectron spectroscopy (XPS) measurements were performed using a Kratos AXIS Ultra HSA with VISION software for data acquisition and CASAXPS software for data analysis. The analysis was carried out with a monochromatic aluminum source (Al Kα = 1487 eV) operating at 15 kV (90 W) in fixed analyzer transmission (FAT) mode, with a pass energy of 40 eV for the regions of interest, and 80 eV for the survey. Data acquisition was performed with a pressure lower than

10^{-6} Pa and using a charge neutralization system. The modeling of the spectra was performed using the XPSPEAK41 program, in which the adjustment of the peaks was performed using peak fitting with Gaussian–Lorentzian peak shape and Shirley type background subtraction.

2.3. Electrochemical Measurements

The electrocatalytic activity of Pt and Pt-RE ($Pt_{0.5}Ce_{0.5}$, $Pt_{0.5}Sm_{0.5}$, $Pt_{0.5}Ho_{0.5}$, $Pt_{0.5}Dy_{0.5}$, and $Pt_{0.4}Dy_{0.6}$) alloy samples for EOR in alkaline medium was studied by cyclic voltammetry (CV), linear scan voltammetry (LSV), and chronoamperometry (CA). Measurements were performed in a 125 mL electrochemical cell using a conventional three-electrode arrangement, where a commercial Pt sheet electrode (Metrohm 6.0305.100) or each of the five Pt-RE alloy electrodes was used as the working electrode, a Johnson Matthey Pt mesh (A $\approx$ 50 cm^2) as the counter electrode, and a Metrohm 6.0701.100 saturated calomel electrode (SCE) as the reference. All the potential values in the paper are referred to in relation to the SCE reference. The working electrode surfaces were polished with a Buehler polishing microcloth pad and rinsed with deionized water before each electrochemical test. The solution temperature inside the cell was controlled by a water jacket in the range 25–45 °C ($\pm$ 0.1 °C) set by a recirculation water bath (Ultraterm 6000383 P-Selecta, Barcelona, Spain). The supporting electrolyte was 2 M NaOH (99 wt.%, AnalaR Normapur), and ethanol concentration (96 % v/v) ranged between 0.2 and 0.8 M.

A PAR 273A computer-controlled potentiostat (Princeton Applied Research, Inc., Oak Ridge, USA) and the associated PowerSUITE software package were used for controlling the experiments and data acquisition. Preliminary tests highlighted the importance of a careful selection of the experimental conditions and measuring procedures: CV, LSV, and CA provided a good response for the EOR experiments, better correlations being obtained with CA at multiple potentials. Each working electrode was pre-activated by applying a potential of −1.1 V for 10 min to ensure the surface was free from oxides. Ethanol oxidation at the six electrodes was first characterized by recording complete CVs by scanning the working electrode potential from the open circuit potential (OCP) up to 0.4 V and back to OCP. LSVs were then run at ten different scan rates, ranging from 5 mV s^{-1} to 1000 mV s^{-1}, from OCP up to 0 V. CA measurements were also done in the 25–45 °C range at potentials ranging from 0 to 0.6 V.

3. Results and Discussion

3.1. Characterization of the Pt-RE Alloys

The SEM micrographs of the 5 prepared Pt-RE alloys are shown in Figure 1a–e, with the data obtained from SEM/EDS characterization being summarized in Figure 1f. The phase composition of the alloys was averaged over several quantitative measurements using different regions of the sample. Two-phase alloys were identified for $Pt_{0.5}Ce_{0.5}$, $Pt_{0.5}Sm_{0.5}$, and $Pt_{0.4}Dy_{0.6}$, with $Pt_{0.5}Ho_{0.5}$ and $Pt_{0.5}Dy_{0.5}$ showing almost single-phase alloy (Figure 1f).

Specifically, the micrographs obtained in backscattered electron (BSE) mode show for $Pt_{0.5}Ce_{0.5}$ alloy (Figure 1a) an equiatomic PtCe grey phase and a Pt_4Ce_3 bright phase at the grain borders. As for $Pt_{0.5}Sm_{0.5}$ alloy, Figure 1b shows an equiatomic PtSm grey phase and a Pt_4Sm_3 bright phase. By opposition, the $Pt_{0.5}Ho_{0.5}$ alloy (Figure 1c) shows an almost homogeneous equiatomic PtHo phase with small amounts of a second phase at the grain borders (not measured). This was also observed for the $Pt_{0.5}Dy_{0.5}$ alloy (Figure 1d), with an almost homogeneous equiatomic PtDy phase with small amounts of a second phase at the grain borders (not measured). On the other hand, the $Pt_{0.4}Dy_{0.6}$ alloy (Figure 1e) shows a Pt_4Dy_5 grey phase and a Pt_3Dy_5 bright phase. It should be noted that the black spots visible in Figure 1d,e are holes.
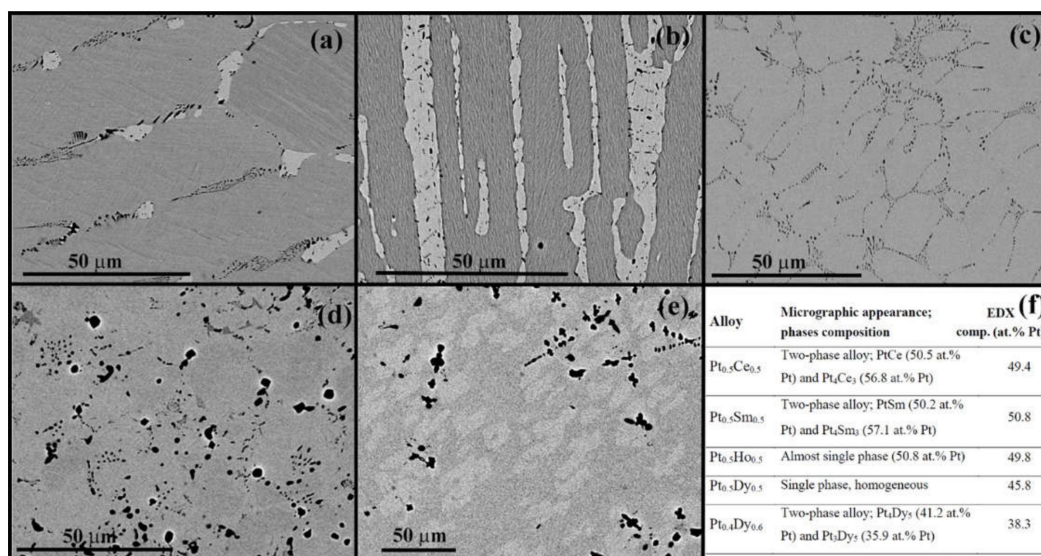
Figure 1. Micrographs (BSE image mode) obtained for (**a**) $Pt_{0.5}Ce_{0.5}$, (**b**) $Pt_{0.5}Sm_{0.5}$, (**c**) $Pt_{0.5}Ho_{0.5}$, (**d**) $Pt_{0.5}Dy_{0.5}$, and (**e**) $Pt_{0.4}Dy_{0.6}$, with (**f**) the corresponding energy dispersive X-ray analysis (EDS) results for each phase. Note: Pt = platinum.

Additionally, XPS analysis was used to study the surface chemical properties of $Pt_{0.5}Sm_{0.5}$, $Pt_{0.5}Ce_{0.5}$, and $Pt_{0.5}Ho_{0.5}$ electrodes. As for the PtDy alloys, severe surface oxidation (following the electrochemical measurements) did not allow a proper XPS analysis to be carried out. Figure 2a shows the Pt 4f region of the spectrum of the Pt-RE alloys; the Pt 4f spectra exhibit two peaks corresponding to Pt $4f_{5/2}$ and Pt $4f_{7/2}$ energy bands, at approximately 75 eV and 71 eV, respectively, which demonstrate the existence of Pt in its metallic state. These spectra also show a similar shape for all Pt-RE catalysts, indicating the same distribution of Pt chemical states for all Pt-RE alloys [129]. Survey data of the mentioned Pt-RE electrodes show the standard lines of each RE element (Figure 2b–d).
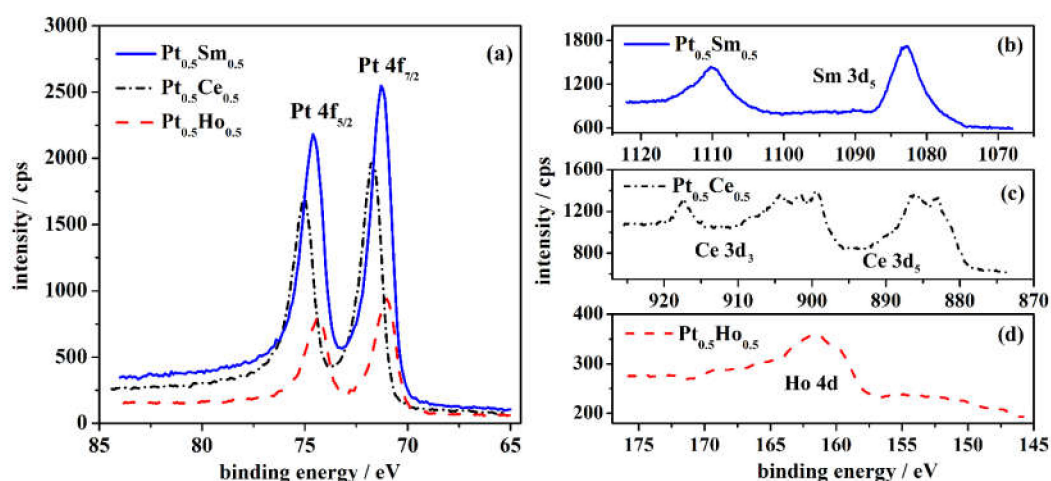

Figure 2. XPS spectra of (**a**) Pt 4f in $Pt_{0.5}Sm_{0.5}$, $Pt_{0.5}Ce_{0.5}$, and $Pt_{0.5}Ho_{0.5}$ and of (**b**) $Pt_{0.5}Sm_{0.5}$, (**c**) $Pt_{0.5}Ce_{0.5}$, and (**d**) $Pt_{0.5}Ho_{0.5}$ alloys in the standard binding energy range of each rare earth (RE) element.

Peaks were observed at binding energies of 1089 to 1073 eV for Sm $3d_5$ (Figure 2b), of 922 to 877 eV for Ce $3d_3$ and Ce $3d_5$ (Figure 2c), and of 174 to 155 eV for Ho 4d (Figure 2d), in agreement with the previously reported standard lines for each RE element [129].

3.2. Electrochemical Properties

Figure 3 displays CVs obtained for ethanol oxidation on Pt-RE alloys, exhibiting the characteristic shape for this process in alkaline medium [130]. The measured OCPs were around −1 V and −0.8 V for Pt and Pt-RE alloy electrodes, respectively. Figure 3a shows the full CVs recorded between OCP and 0.4 V. Generally, the CVs were composed of a well-defined anodic peak around –0.4 V and, in the reverse scan, a cathodic peak around the same potential. However, when the potential is scanned only from the OCP until 0 V, the cathodic peak vanishes, and a reoxidation peak appears instead, at around −0.4 V (Figure 3b). This reoxidation peak might be related to the reactivation of the electrode surface for ethanol oxidation at potentials below 0 V, or it may be due to the oxidation of surface adsorbed intermediates formed in the anodic scan direction. Figure 3a clearly shows that all the Pt-RE alloys show better performance for EOR in the alkaline medium than the Pt electrode, the highest values of the peak current density, j_p, being obtained with the $Pt_{0.5}Sm_{0.5}$ electrode.
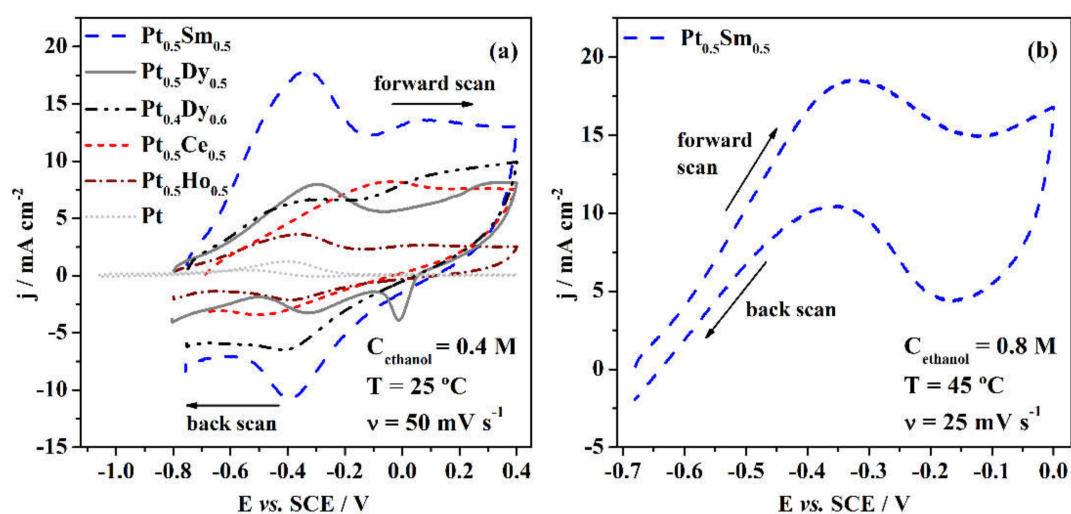

Figure 3. Cyclic voltammograms (CV) of (**a**) Pt and Pt-RE alloys in 0.4 M ethanol + 2 M NaOH at 50 mV s^{-1} and 25 °C and shorter-range CV of (**b**) $Pt_{0.5}Sm_{0.5}$ electrode in 0.8 M ethanol + 2 M NaOH at 25 mV s^{-1} and 45 °C.

Similar conclusions have been reported by other workers [48,61,116,117,122] that studied Pt- and Pt-RE-based binary and ternary alloys for the electrooxidation of ethanol. In general, they agree that these alloys show superior performance in terms of activity and stability than bare Pt electrodes. The incorporation of small amounts of REs is largely evaluated in terms of electronic effects. For example, Corradini et al. [116] attribute the presence of REs to the emptying of the PtL_3 band due to an electronic transition from the Pt 5d orbital to the RE 4f orbital, that weakens the adsorption of intermediate products by Pt, favoring the bifunctional EOR mechanism, since the RE renders oxygenated species available at lower potentials.

Then, LSVs were recorded at different potential scan rates, v, in the 5–1000 mV s^{-1} range. In general, an anodic shift of the peak potential, E_p, with the increase of v was observed, typical of electrochemical irreversible processes [126,131]. However, the LSVs recorded for Pt and $Pt_{0.5}Dy_{0.5}$ electrodes showed a different behavior, in which there was an insignificant change of E_p with v, usually ascribed to a reversible electrochemical process. Figure 4 shows a direct comparison between the LSVs recorded in 0.8 M ethanol solution at 35 °C for Pt and for the $Pt_{0.5}Sm_{0.5}$ electrode, where the latter clearly shows the E_p anodic shift with the v increase (Figure 4a), whereas E_p remains relatively constant for the Pt electrode (Figure 4b). It should be noted that due to the high number of different experimental conditions (6 electrode materials × 3 temperatures (25, 35, and 45 °C) × 3 ethanol concentrations (0.2, 0.4, and 0.8 M) = 54), representative results have been selected for presentation in Figure 4.

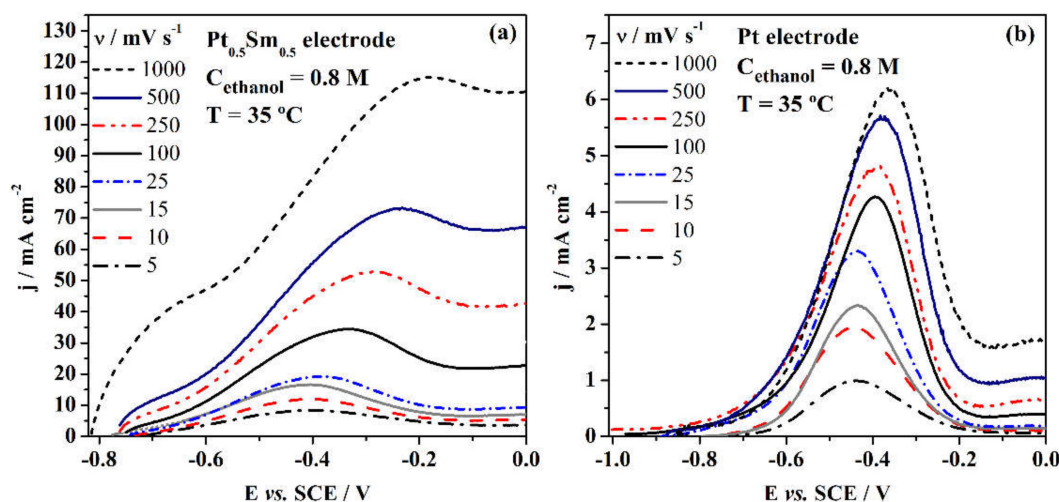**Figure 4.** Anodic polarization curves of (**a**) $Pt_{0.5}Sm_{0.5}$ electrode and (**b**) Pt electrode in 0.8 M ethanol + 2 M NaOH, at 35 °C, for ν ranging from 5 to 1000 mV s^{-1}.

The dependences of the peak current density on the square root of the scan rate and the peak potential on the logarithm of scan rate were found to be relatively linear for most Pt-RE electrodes, confirming the irreversible nature of the electrode processes. Figure 5a shows the E_p vs. ln ν plot for $Pt_{0.5}Ho_{0.5}$ electrode in 0.2 M ethanol solution at 25 °C, and Figure 5b shows the corresponding j_p vs. $ν^{1/2}$ plot.
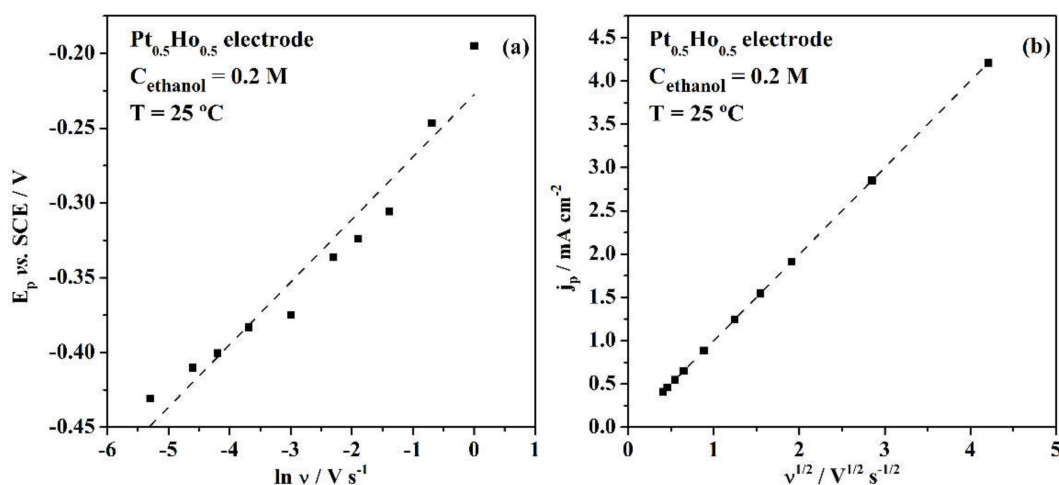

Figure 5. (**a**) E_p vs. ln ν and (**b**) j_p vs. $ν^{1/2}$ plots for $Pt_{0.5}Ho_{0.5}$ electrode in 0.2 M ethanol + 2 M NaOH, at 25 °C.

From the slope of the E_p vs. ln ν plots (Figure 5a) and by application of Equation (10) [132], it is possible to calculate the anodic charge transfer coefficients α,

$$E_p = E^0 + \left\{ \frac{RT}{(1-\alpha)n_aF} \right\} \times \left\{ 0.78 + \ln\left(\frac{D}{k_s}\right) + \ln\left[\frac{(1-\alpha)n_aFν}{RT} \right]^{1/2} \right\} \tag{10}$$

where R is the universal gas constant (8.314 J K^{-1} mol^{-1}), T is the temperature (K), D is the diffusion coefficient (cm^2 s^{-1}), k_s is the standard heterogeneous rate constant (cm s^{-1}), n_a is the number of electrons involved in the rate-determining step (normally 1), and F is Faraday's constant (96,485 C mol^{-1}).

To get α from Equation (10), it was first necessary to obtain the ethanol diffusion coefficient, D, in 2 M NaOH solutions. The ethanol D values can be obtained by the application of Equation (11), following chronoamperometric (CA) measurements at a microdisk electrode. The method has the advantage of obtaining D without previous knowledge of the number of exchanged electrons in EOR, as required by the typical Cottrell equation [133,134].

Therefore, CA measurements were performed using a gold (Au) microdisk electrode for applied potentials ranging from 0 to 0.6 V at 25, 35, and 45 °C. Results were then linearized regarding the steady-state current, $i_{d,ss}$, by plotting $i_d/i_{d,ss}$ vs. $t^{-1/2}$. Figure 6a shows the CA curves obtained at 25 °C for each applied electrode potential, and Figure 6b shows the corresponding linearization of the CA curves obtained at 0.5 V for the three tested temperatures.
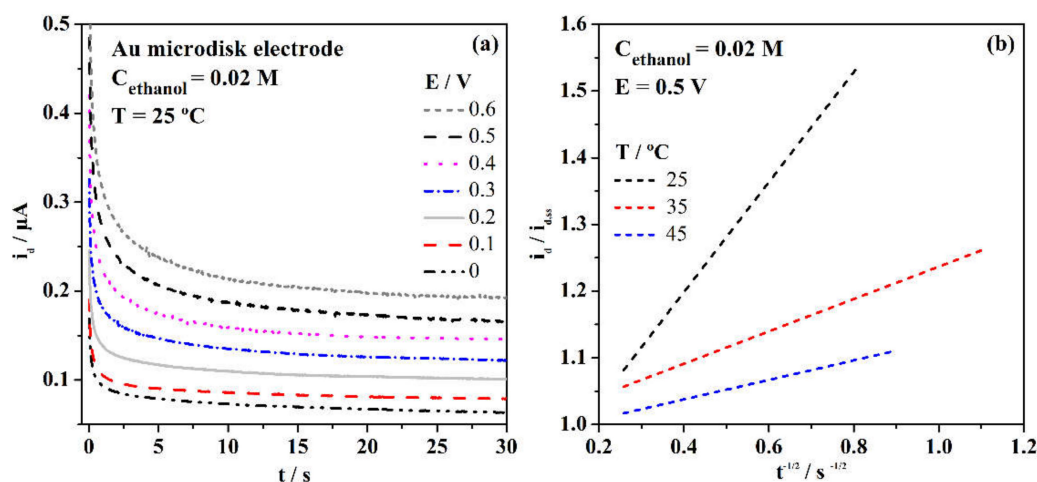

Figure 6. (**a**) Current transients following application of potentials in the 0–0.6 V range in 0.02 M ethanol + 2 M NaOH solution at 25 °C and (**b**) $i_d/i_{d,ss}$ vs. $t^{-1/2}$ plots for an applied potential of 0.5 V at 25, 35, and 45 °C.

From the slope of the plots shown in Figure 6b, it is possible to determine the D values by direct application of Equation (11) [133],

$$i_d/i_{d,ss} = (\pi^{1/2}/4)\, a\, (Dt)^{-1/2} + 1 \tag{11}$$

where i_d is the diffusion current, $i_{d,ss}$ is the diffusion current in the steady-state and a is the radius of the Au microdisk electrode (12.5×10^{-4} cm). $i_{d,ss}$ values were taken directly from Figure 6a at 30 s, after stabilization of the recorded currents. Time ranges between ca. 1 s and 16 s allowed a good linearization of the $i_{d,ss}$ vs. $t^{-1/2}$ plots (Figure 6b). Thus, ethanol D values were evaluated to be 2.64×10^{-6}, 5.21×10^{-6}, and 1.41×10^{-5} cm^2 s^{-1} at 25, 35, and 45 °C, respectively. The values show a significant increase with the solution temperature, as expected. The calculated Ds could then be applied to determine the charge transfer coefficients, α, and the number of exchanged electrons, n, in EOR.

Accordingly, by application of Equation (10), α values were determined for ethanol concentrations of 0.2, 0.4, and 0.8 M in the 25–45 °C temperature range. Average α values were found to be 0.60, 0.64, and 0.69 for $Pt_{0.5}Ho_{0.5}$, $Pt_{0.5}Sm_{0.5}$, and $Pt_{0.4}Dy_{0.6}$ electrodes, respectively. The α values obtained for $Pt_{0.5}Ho_{0.5}$ and $Pt_{0.5}Sm_{0.5}$ alloys show that it tends to slightly decrease with the increase of ethanol concentration, whereas the $Pt_{0.4}Dy_{0.6}$ alloy shows the opposite trend. Results also show a negligible effect of the temperature on α. Additionally, the $Pt_{0.5}Ce_{0.5}$ electrode revealed poor stability due to pronounced surface oxidation following the LSV measurements, leading the material to fall off the support. For that reason, $Pt_{0.5}Ce_{0.5}$ alloy was not considered for subsequent studies. This situation was not observed with the other tested Pt-RE electrodes. Although it is not fully proven that they are

very stable, all the tests carried out for their evaluation suggest good stability behavior. It should be emphasized that apart from the electrocatalytic activity, lifespan and stability are crucial parameters for electrodes, catalysts, and catalyst supports for fuel cell applications. Chronoamperometry, repetitive potential cycling, linear scan, and derivative voltammetry, along with other ex-situ and in situ experiments, have been employed to evaluate the EOR short-term stability, short-term durability, and long-term structural durability. Short-term stability, usually evaluated by chronoamperometry, is the ability to recover the activity lost during continuous operation. For example, poisoning of active electrode surfaces by fuel contaminants or intermediate species by fuel cell reactions, and reversible material changes explain a great part of these catalytic activity decays. Short-term durability is the catalyst's ability to resist permanent change in performance over time. Durability decay is due to loss of electrochemical surface area, loss of co-catalyst, carbon corrosion, etc., is related to aging. Long-term structural durability is one of the characteristics most necessary for fuel cells to be accepted as a viable product. The durability of the EOR catalysts is usually evaluated by repetitive potential cycling under an Ar atmosphere and/or CO atmosphere. Information about the stability of the electrodes is not as common as about their catalytic activity, but there are some published stability studies on the EOR/DEFC by Pt-RE materials [51,111,112,115,118,123].

From the slope of the j_p vs. $\nu^{1/2}$ plots (Figure 5b), and using the previously calculated α and D values, it is now possible to obtain the number of electrons, n, exchanged in EOR by employing Equation (12), valid for the irreversible electrochemical processes, where j_p is the peak current density in A cm^{-2} and C is the ethanol concentration in M. As mentioned previously, the insignificant change of E_p with ν for the LSVs recorded at Pt (Figure 4b) and $Pt_{0.5}Dy_{0.5}$ electrodes is typical of reversible processes, which require that n at those two electrodes be determined by the application of the classical Randles–Sevcik equation (Equation (13)) [132].

$$j_p = 2.99 \times 10^5 [(1-\alpha) \times n_a]^{1/2} nC(D\nu)^{1/2} \tag{12}$$

$$j_p = 0.4463 \left(\frac{F^3}{RT}\right)^{1/2} n^{3/2} C(D\nu)^{1/2} \tag{13}$$

Despite the recorded high currents, the average number of exchanged electrons, n, obtained in 0.2 M ethanol was considerably low, being 0.2 for $Pt_{0.5}Ho_{0.5}$, 0.7 for $Pt_{0.5}Sm_{0.5}$, 0.4 for $Pt_{0.5}Dy_{0.5}$, 0.2 for $Pt_{0.4}Dy_{0.6}$, and 0.06 for Pt. In agreement with the CV results, the $Pt_{0.5}Sm_{0.5}$ alloy led to the highest n values, whereas Pt had the lowest. The solution temperature does not seem to have a clear effect on the calculated n. On the other hand, the increase in ethanol concentration leads to a large decrease in the EOR n values, possibly due to a decrease in reaction efficiency. It is predicted that higher n values could be obtained at lower ethanol concentrations, although that would be meaningless for application in a practical DEFC, where the ethanol concentration can be as high as 2 M. The EOR reaction order at the Pt and Pt-RE electrodes can be determined by the application of Equation (14),

$$j_p = z\, C^\beta \tag{14}$$

where β is the reaction order, and z is a constant.

Therefore, by running LSVs at different ethanol concentrations, the β values could be obtained from the slope of the ln j_p vs. ln C plots. Figure 7 shows the voltammograms obtained at 50 mV s^{-1} using a Pt electrode at 45 °C, and for ethanol concentrations of 0.2, 0.4, and 0.8 M. The inset shows the corresponding ln j_p vs. ln C plot for calculation of the EOR reaction order at the Pt electrode. The average reaction orders for the $Pt_{0.5}Ho_{0.5}$, $Pt_{0.5}Sm_{0.5}$, $Pt_{0.5}Dy_{0.5}$, $Pt_{0.4}Dy_{0.6}$, and Pt electrodes were 0.9, 0.4, 0.4, 0.4, and 0.7, respectively.
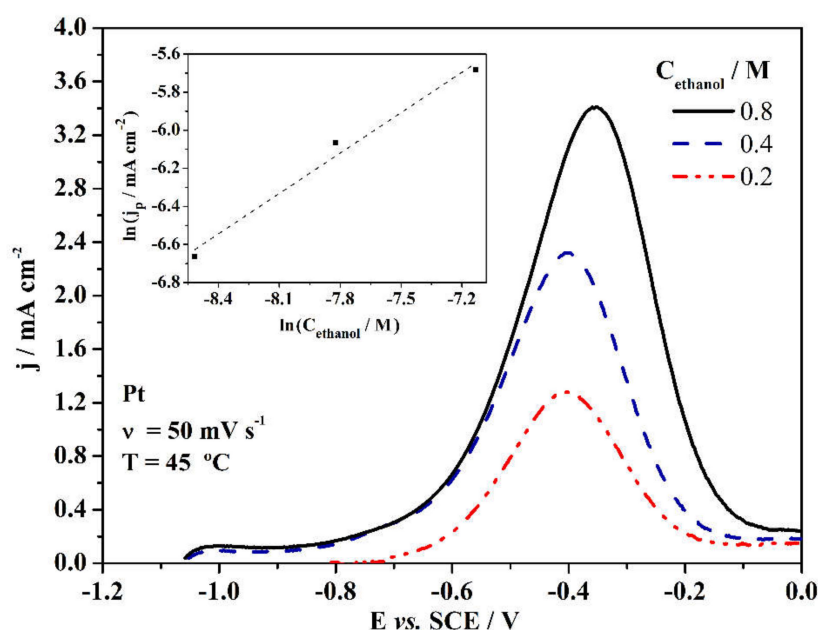
Figure 7. Effect of ethanol concentration (0.2–0.8 M) on the anodic scans of Pt electrode at 50 mV s^{-1} and 45 °C. Inset shows the corresponding ln j$_p$ vs. ln C plot used for determining the reaction order.

Based on this kinetic parameter, and considering that the reaction order depends essentially on the mechanism of the EOR and its ethanol concentration (as long as the other experimental conditions are the same), it can be concluded that the average reaction orders for the Pt and Pt$_{0.5}$Ho$_{0.5}$ electrodes are relatively similar, so that the reaction mechanism for these materials is the same. If the rate constant for the five tested electrodes is exclusively dependent on the product species for which it was calculated, its average value of 0.4 for the other 3 electrodes means that their rate constants are lower than the rate constants for Pt and Pt$_{0.5}$Ho$_{0.5}$. However, this conclusion is in contrast with the other observations that suggest, for example, that the Pt$_{0.5}$Sm$_{0.5}$ is the most electroactive material. It seems that the studied electrodes have not the same kinetic mechanism, being necessary to perform further studies to properly explain this issue. Nevertheless, the overview of the research background and the results reported in this work show that the kinetics of EOR is very complex and requires further theoretical and experimental studies. It is believed that the present results and corresponding reasoning contribute to the solution to this energy problem.

4. Conclusions

In this work, the ethanol oxidation reaction (EOR) has been studied at Pt-RE electrodes by cyclic and linear scan voltammetry as a function of the alcohol concentration (0.2–0.8 M) and the working temperature (25–45 °C). The voltammograms recorded between OCP and 0 V vs. SCE show an anodic peak in the progressive scan and a second anodic peak in the regressive scan. When extending the CV electroactivity domain, a clear reduction peak is observed in the regressive scan, which may be the result of further oxidation of the electrode materials at anodic potentials well over 0 V. The first anodic peak shows that peak current densities increase with the potential scan rate for all the tested materials. Values of peak potential also vary with increasing scan rates for most Pt-RE electrodes but are almost constant for the Pt$_{0.5}$Dy$_{0.5}$ and Pt electrodes in all tested conditions. From these data, it is possible to conclude that EOR is an irreversible process in four of the Pt-RE alloys, being a quasi-reversible process in Pt$_{0.5}$Dy$_{0.5}$ and Pt electrodes. Ethanol diffusion coefficients of ca. 10^{-6}–10^{-5} cm^2 s^{-1} were determined by chronoamperometry. Anodic charge transfer coefficients varied between 0.60 and 0.69, and reaction orders ranged between 0.4 and 0.9. The Pt$_{0.5}$Sm$_{0.5}$ electrode showed the highest activity for EOR. From the electrochemical experiments, it is evident that independent of the electrolyte

concentration and catalyst composition, all the Pt-RE electrodes led to higher current densities than the modest ones displayed by Pt. This is particularly interesting from the DEFCs point of view because it can increase the cell energy density of DEFC systems and, consequently, their operation power density. It is suggested that the differences observed in the electrodes are mainly due to different kinetics of the oxidation reaction, which encourages further studies of their divergent behaviors occurring at the electrochemical level, being also necessary to confirm their long-term stability.

References

1. Dyer, C.K. Fuel cells for portable applications. *J. Power Sources* **2002**, *106*, 31–34. [CrossRef]
2. Yao, L.; Chang, Y. Shaping China's energy security: The impact of domestic reforms. *Energy Policy* **2015**, *77*, 131–139. [CrossRef]
3. Töpler, J.; Lehmann, J. *Hydrogen and Fuel Cell: Technologies and Market Perspectives*; Springer: Berlin/Heidelberg, Germany, 2016.
4. Stolten, D.; Samsun, R.C.; Garland, N. *Fuel Cells: Data, Facts and Figures*; Wiley-VCH Verlag GmbH & Co. KGaA: Weinheim, Germany, 2016.
5. Marken, F.; Fermin, D. *Electrochemical Reduction of Carbon Dioxide: Overcoming the Limitations of Photosynthesis*; RSC: Cambridge, UK, 2018.
6. Qiao, J.; Liu, Y.; Hong, F.; Zhang, J. A review of catalysts for the electroreduction of carbon dioxide to produce low-carbon fuels. *Chem. Soc. Rev.* **2014**, *43*, 631–675. [CrossRef] [PubMed]
7. Hirschenhofer, J.H.; Stanfer, D.B.; Engleman, R.R.; Klett, M.G. *Fuel Cell Handbook*, 4th ed.; FETC: Morgantown, WV, USA, 1998.
8. Vielstich, W.; Lamm, A.; Gasteiger, H.A. *Handbook of fuel Cells: Fundamentals, Technology and Applications*; John Wiley & Sons Ltd.: Chichester, UK, 2003.
9. Hartl, F.W.; Varela, H. The effect of solution pH and temperature on the oscillatory electro-oxidation of formic acid on platinum. *Chem. Sel.* **2017**, *2*, 8679–8685. [CrossRef]
10. Maiyalagan, T.; Saji, V.S. *Electrocatalysts for Low Temperature Fuel Cells: Fundamentals and Recent Trends*; Wiley-VCH: Weinhein, Germany, 2017.
11. Sarma, S.C.; Peter, S.C. Understanding small-molecule electro-oxidation on palladium based compounds—A feature on experimental and theoretical approaches. *Dalton Trans.* **2018**, *47*, 7864–7869. [CrossRef] [PubMed]
12. Tripković, D.V.; Popović, K.D.; Jovanović, V.M.; Nogueira, J.A.; Varela, H.; Lopes, P.P.; Strmcnik, D.; Stamenkovic, V.R.; Markovic, N.M. Tuning of catalytic properties for electrooxidation of small organic molecules on Pt-based thin films via controlled thermal treatment. *J. Catal.* **2019**, *371*, 96–105. [CrossRef]
13. Zheng, Y.; Wan, X.; Cheng, X.; Cheng, K.; Dai, Z.; Liu, Z. Advanced catalytic materials for ethanol oxidation in direct ethanol fuel cells. *Catalysts* **2020**, *10*, 166. [CrossRef]
14. Yun, Y. Alcohol Fuels: Current status and future direction. *IntechOpen* **2020**. Available online: https://www.intechopen.com/online-first/alcohol-fuels-current-status-and-future-direction (accessed on 29 January 2020). [CrossRef]
15. Bahrami, H.; Faghai, A. Exergy analysis of a passive direct methanol fuel cell. *J. Power Sources* **2011**, *196*, 1191–1204. [CrossRef]
16. Zhao, T.S.; Yang, W.W.; Chan, R.; Wu, Q.X. Towards operating direct methanol fuel cells with highly concentrated fuel. *J. Power Sources* **2010**, *195*, 3451–3462. [CrossRef]

17. Yu, E.H.; Krewer, U.; Scott, K. Principles and materials aspects of direct alkaline alcohol fuel cells. *Energies* **2010**, *3*, 1499–1528. [CrossRef]

18. Liang, Z.X.; Zha, T.S. *Catalysts for Alcohol Fuelled Direct Oxidation Fuel Cells*; RSC: Cambridge, UK, 2012.

19. Yavari, Z.; Noroozifar, M.; Khorasani-Motlagh, M.; Roodbaneh, M.M.; Ajorlou, B. $SrFeO_{3-x}$ assisting with Pd nanoparticles on the performance of alcohols catalytic oxidation. *Iran. J. Chem. Chem. Eng.* **2017**, *36*, 21–37.

20. Gurau, B.; Smotkin, E.S. Methanol crossover in direct methanol fuel cells: A link between power and energy density. *J. Power Sources* **2002**, *112*, 339–352. [CrossRef]

21. Alizadeh, E.; Farhadi, M.; Sedighi, K.; Shakeri, M. The effect of cell temperature and channel geometry on the performance of a direct methanol fuel cell. *J. Fuel Cell Sci. Technol.* **2013**, *10*, 031002. [CrossRef]

22. Yuan, Z.Y.; Yang, J. The effect of temperature on the output characteristics of micro direct methanol fuel cell. *J. Power Sources* **2015**, *285*, 318–324. [CrossRef]

23. Badwal, S.P.S.; Giddy, S.; Kulkarni, A.; Goel, J.; Basu, S. Direct ethanol fuel cells for transport and stationary applications. A comprehensive review. *Appl. Energy* **2015**, *145*, 80–103. [CrossRef]

24. Lamy, C.; Coutanceau, C. Electrocatalysis of alcohol oxidation reactions at platinum group metals. In *Catalysts for Alcohol Fuelled Direct Oxidation Fuel Cells*; Liang, Z.X., Zhao, T.S., Eds.; RSC: Cambridge, UK, 2012; pp. 1–70.

25. Vigier, F.; Rousseau, S.; Coutanceau, C.; Leger, J.-M.; Lamy, C. Electrocatalysis for the direct alcohol fuel cell. *Top. Catal.* **2006**, *40*, 111–121. [CrossRef]

26. Du, W.; Wang, Q.; Saxner, D.; Deskins, N.A.; Su, D.; Krzanowski, J.E.; Frenkel, A.I.; Teng, X. Highly active iridium/iridium à tin/tin oxide heterogeneous nanoparticles as alternative electrocatalysts for the ethanol oxidation reaction. *J. Am. Chem. Soc.* **2011**, *133*, 15172–15183. [CrossRef]

27. Li, M.; Guo, W.; Jiang, R.; Zhao, L.; Shan, H. Decomposition of ethanol on Pd (111): A density functional theory study. *Langmuir* **2010**, *26*, 1879–1888. [CrossRef]

28. Alcala, R.; Shabaker, J.W.; Huber, J.W.; Sanchez-Castillo, M.A.; Dumesic, J.A. Experimental and DFT studies of ethanol and acetic acid on Pt-Sn based catalysts. *J. Phys. Chem. B* **2005**, *109*, 2074–2085. [CrossRef]

29. Alcala, R.; Mavrikakis, M.; Dumesic, J.A. DFT studies for cleavage of C-C and C-O bonds in surface species derived from ethanol on Pt (111). *J. Catal.* **2003**, *218*, 178–190. [CrossRef]

30. Xin, H.; Holewinski, A.; Schweitzer, N.; Nikolla, E.; Linic, S. Electronic structure engineering in heterogeneous catalysis: Identified novel alloy catalysts based on rapid screening for materials with desired electronic properties. *Top. Catal.* **2012**, *55*, 376–390. [CrossRef]

31. Ferrin, P.; Simonetti, D.; Kandoi, S.; Kunkes, E.; Dumesic, J.A.; Norskov, J.K.; Mavrikakis, M. Modeling ethanol decomposition on transition metals: A combined application of scaling and Bronsted-Evans-Polanyi relations. *J. Am. Chem. Soc.* **2009**, *131*, 5809–5815. [CrossRef] [PubMed]

32. Cao, B.I.; Sun, G.; Li, H.; Xin, Q. Carbon supported IrSn Catalysts for direct ethanol fuel cell. *Fuel Cells Bull.* **2007**, *2007*, 12–16. [CrossRef]

33. Du, W.; Deskins, N.A.; Su, D.; Teng, X. Iridium-ruthenium alloyed nanoparticles for the ethanol oxidation. *ACS Catal.* **2012**, *2*, 1226–1231. [CrossRef]

34. Zhou, W.; Zhou, Z.; Song, S.; Li, W. Pt based anode catalysts for direct ethanol fuel cells. *Appl. Catal. B Environ.* **2003**, *46*, 273–285. [CrossRef]

35. Colmenares, L.; Wang, H.; Jusys, Z.; Jiang, J.; Yan, S.; Sun, G.Q.; Behm, R.J. Ethanol oxidation on novel carbon supported Pt alloy catalysts—Model studies under defined diffusion conditions. *Electrochim. Acta* **2006**, *52*, 221–233. [CrossRef]

36. Lamy, C.; Rousseau, S.; Belgsir, E.M.; Coutanceau, C.; Leger, C. Recent Progress in the direct ethanol fuel cell: Development of new platinum-tin electrocatalysts. *Electrochim. Acta* **2004**, *49*, 3901–3908. [CrossRef]

37. Vigier, F.; Coutanceau, C.; Leger, J.-H.; Perrard, A.; Belgsia, E.M.; Lamy, C. Development of anode catalysts for a direct etanol fuel cell. *J. Appl. Electrochem.* **2004**, *34*, 439–446. [CrossRef]

38. Yovanovich, M.; Piasentin, R.M.; Ayoub, J.M.S.; Nandenha, J.; Fontes, E.H.; De Souza, R.F.B.; Buzzo, G.S.; Silva, J.C.M.; Spinace, E.V.; Assumpção, M.H.M.T.; et al. Pt Bi/C electrocatalysts for formic acid electrooxidation in acid and alkaline electrolytes. *Int. J. Electrochem. Sci.* **2015**, *10*, 4801–4811.

39. Wang, Y.; Zou, S.; Cai, W.B. Recent advances on electrooxidation of ethanol on Pt- and Pd-based electrocatalysts: From reaction mechanisms to catalytic materials. *Catalysts* **2015**, *5*, 1507–1534. [CrossRef]

40. Xie, W.; Zhang, F.; Wang, Z.; Yang, M.; Xia, J.; Gui, R.; Xia, Y. Facile preparation of PtPdPt/graphene nanocomposites with ultrahigh electrocatalytic performance for methanol oxidation. *J. Electroanal. Chem.* **2016**, *761*, 55–61. [CrossRef]

41. Soares, L.A.; Morais, C.; Napporn, T.W.; Kokoh, K.B.; Olivi, P. Beneficial effects of rhodium and tin oxide on carbon supported platinum catalysts for ethanol electrooxidation. *J. Power Sources* **2016**, *315*, 47–55. [CrossRef]

42. Ocampo-Restrepo, V.K.; Calderón-Cárdenas, A.; Lizcano-Valbuena, W.H. Catalytic activity of Pt-based nanoparticles with Ni and Co for ethanol and acetaldehyde electrooxidation in alkaline medium. *Electrochim. Acta* **2017**, *246*, 475–483. [CrossRef]

43. He, C.; Desai, S.; Brown, G.; Bollepallic, S. PEM fuel cell catalysts: Cost, performance and durability. *Electrochem. Soc. Interfaces* **2005**, *14*, 41–44.

44. Li, B.; Qiao, J.; Yang, D.; Lin, R.; Lv, H.; Wang, H.; Ma, J. Effect of metal particle size and Nafion content on performance of MEA using Ir-V/C as anode catalyst. *Int. J. Hydrog. Energy* **2010**, *35*, 5528–5538. [CrossRef]

45. De Souza, J.P.I.; Queiroz, S.L.; Bergamaski, K.; Gonzalez, E.R.; Nart, F.C.; De Sa, U. SpC Electrooxidation of ethanol on Pt, Rh and PtRh electrodes. A Study using DEMS and in-situ FTIR techniques. *J. Phys. Chem. B* **2002**, *106*, 9825–9830. [CrossRef]

46. Alayoglu, S.; Nilekar, A.U.; Mavrikakis, M.; Eichhorn, B. Ru-Pt core-shell nanoparticles for preferential oxidation of carbon monoxide in hydrogen. *Nat. Mater.* **2008**, *7*, 333–338. [CrossRef]

47. Su, H.-Y.; Gu, X.-K.; Ma, X.; Zhao, Y.-X.; Bao, X.-H.; Li, W.-X. Structure evolution of Pt-3d transition metal alloys under reductive and oxidizing conditions and effect on the CO oxidation: A first principles study. *Catal. Today* **2011**, *165*, 89–95. [CrossRef]

48. Antolini, E. Catalysts for direct ethanol fuel cells. *J. Power Sources* **2007**, *170*, 1–12. [CrossRef]

49. Leger, J.; Rousseau, S.; Coutanceau, C.; Hahn, F.; Lamy, C. How bimetallic electrocatalysts does work for reaction involved in fuel cells? Example of ethanol oxidation and comparison to methanol. *Electrochim. Acta* **2005**, *50*, 5118–5125. [CrossRef]

50. Ju, K.-S.; Pak, S.-N.; Ri, C.-N.; Ryo, H.-S.; Kim, K.-I.; So, S.-R.; Ri, C.-K.; Ri, S.-P.; Nam, K.-W.; Pak, K.-S.; et al. Ethanol electrooxidation on carbon-supported Pt_1Mn_3 catalyst investigated by pinhole on-line electrochemical mass spectrometry. *Chem. Phys. Lett.* **2019**, *727*, 78–84. [CrossRef]

51. Matin, M.A.; Kumar, A.; Saad, M.A.H.S.; Al-Marri, M.J.; Suslou, S. Zn-enriched PtZn nanoparticle electrocatalysts synthesized by solution combustion for ethanol oxidation reaction in an alkaline medium. *MRS Commun.* **2018**, *8*, 411–419. [CrossRef]

52. Raoof, J.-B.; Hosseini, S.R.; Rezaee, S. Preparation of Pt/Poly (2-Methoxyaniline)—Sodium dodecyl sulfate composite and its application for electrocatalytic oxidation of methanol and formaldehyde. *Electrochim. Acta* **2014**, *141*, 340–348. [CrossRef]

53. Zhang, Y.; Chang, G.; Shu, H.; Oyama, H.; Liu, X.; He, Y. Synthesis of Pt-Pd bimetallic nanoparticles anchored on graphene for highly active methanol electrooxidation. *J. Power Sources* **2014**, *262*, 278–285. [CrossRef]

54. Zhu, H.; Li, G.; Lv, X.; Zhao, Y.; Huang, T.; Liu, H.; Li, J. Controlled synthesis of hierarchical tetrapod Pd nanocrystal and their enhanced electrocatalytic properties. *RSC Adv.* **2014**, *4*, 6535–6539. [CrossRef]

55. Hathoot, A.A. Electrooxidation of iodide ion at poly 8-(3-acetylimino-6 methyl-2,4-dioxopyran)-1-aminonaphthalene modified electrode in aqueous solution. *Croat. Chem. Acta* **2011**, *84*, 469–473. [CrossRef]

56. Hathoot, A.A.; Yousef, U.S.; Shatla, A.S.; Abdel-Azzem, M. Simultaneous determination of ascorbic acid, uric acid and dopamine at modified electrode based on hybrid nickel hexacyanoferrate/poly (1,5 diaminonaphtalene). *J. Iran. Chem. Soc.* **2017**, *14*, 1789–1799. [CrossRef]

57. Liu, L.; Pippel, E.; Scholz, R.; Gosele, U. Nanoporous Pt-Co alloy nanowires: Fabrication, characterization and electrocatalytic properties. *Nano Lett.* **2009**, *9*, 4352–4358. [CrossRef]

58. Greeley, J.; Mavrikakis, M. Alloy catalysts designed from first principles. *Nat. Mater.* **2004**, *3*, 810–815. [CrossRef]

59. Nilekar, A.U.; Alayoglu, S.; Eichhorn, B.; Mavrikakis, M. Preferential CO oxidation in hydrogen: Reactivity of core-shell nanoparticles. *J. Am. Chem. Soc.* **2010**, *132*, 7418–7428. [CrossRef] [PubMed]

60. Schmidt, V.M.; Ianniello, R.; Pastor, E.; González, S. Electrochemical reactivity of ethanol on porous Pt and PtRu: Oxidation/reduction reactions in 1 M $HClO_4$. *J. Phys. Chem.* **1996**, *100*, 17901–17908. [CrossRef]

61. Colmati, F.; Antolini, E.; Gonzalez, E.R. Effect of temperature on the mechanism of ethanol oxidation on carbon supported Pt, PtRu and Pt_3Sn electrocatalysts. *J. Power Sources* **2006**, *157*, 98–103. [CrossRef]

62. Rutkowska, I.A.; Koster, M.D.; Blanchard, G.J.; Kulesza, P.J. Enhancement of ethanol oxidation at Pt and PtRu nanoparticles dispersed over hybrid zirconia-rhodium supports. *J. Power Sources* **2014**, *272*, 681–688. [CrossRef]

63. Rutkowska, I.A.; Kulesza, P.J. Electroanalysis of ethanol oxidation reactivity of platinum-ruthenium catalysts supported onto nanostructured titanium dioxide matrices. *J. Electrochem. Soc.* **2016**, *163*, H3052–H3060. [CrossRef]

64. Asgardi, J.; Calderón, J.C.; Alcaide, F.; Querejeta, A.; Calvillo, L.; Lázaro, M.J.; Garcia, J.; Pastor, E. Carbon monoxide and ethanol oxidation on PtSn supported catalysts: Effect of the nature of the carbon support and Pt: Sn composition. *Appl. Catal. B Environ.* **2015**, *168*, 33–41. [CrossRef]

65. Rizo, R.; Sebastian, D.; Lazaro, M.J.; Pastor, E. On the design of Pt-Sn efficient catalyst for carbon monoxide and ethanol oxidation in acid and alkaline media. *Appl. Catal. B Environ.* **2017**, *200*, 246–254. [CrossRef]

66. Zhou, W.J.; Li, W.Z.; Song, S.Q.; Zhou, Z.H.; Jiang, L.H.; Sun, G.Q.; Xin, Q.; Poulianitis, K.; Kontou, S.; Tsiakaras, P. Bi-and tri-metallic Pt-based anode catalysts for direct ethanol fuel cells. *J. Power Sources* **2004**, *131*, 217–223. [CrossRef]

67. Ghavidel, M.Z.; Easton, E.B. Improving the ethanol oxidation activity of Pt-Mn alloys through the use of additives during deposition. *Catalysts* **2015**, *5*, 1016–1033. [CrossRef]

68. Zhang, Q.; Mellinger, Z.J.; Jiang, Z.; Chen, X.; Wang, B.; Tian, B.; Liang, Z.; Chen, J.G. Palladium-modified tungsten carbide for ethanol electrooxidation: From surface science studies to electrochemical evaluation. *J. Electrochem. Soc.* **2018**, *165*, J3031–J3038. [CrossRef]

69. Mukherjee, P.; Bagchi, J.; Dutta, S.; Bhattacharia, S.K. The nickel supported platinum catalyst for anodic oxidation of ethanol in alkaline medium. *Appl. Catal. A-Gen.* **2015**, *506*, 220–227. [CrossRef]

70. Ottoni, C.A.; Ramos, C.E.D.; de Souza, R.F.B.; da Silva, S.G.; Spinace, E.V.; Neto, A.O. Glycerol and ethanol oxidation in alkaline medium using PtCu/C electrocatalysts. *Int. J. Electrochem. Sci.* **2018**, *13*, 1893–1904. [CrossRef]

71. Delpeuch, A.B.; Maillard, F.; Chatenet, M.; Soudant, P.; Cremers, C. Ethanol oxidation reaction (EOR) investigation on Pt/C, Rh/C, and Pt-based bi- and tri-metallic electrocatalysts: A DEMS and in situ FTIR study. *Appl. Catal. B Environ.* **2016**, *181*, 672–680. [CrossRef]

72. Hassan, K.M.; Hathoot, A.A.; Maher, R.; Azzen, M.A. Electrocatalytic oxidation of ethanol at Pd, Pt, Pd/Pt and Pt/Pd nanoparticles supported on poly 1,8 diaminonaphthalene film in alkaline medium. *RSC Adv.* **2018**, *8*, 15417–15426. [CrossRef]

73. Amorim, A.; Parreira, L.S.; Silva, J.C.M.; dos Santos, M.C. Electrooxidation of mixed ethanol and methanol solutions on PtSn/C electrocatalysts prepared by the polymeric precursor method. *J. Braz. Chem. Soc.* **2017**, *28*, 1091–1097. [CrossRef]

74. Gu, Z.; Li, S.; Xiong, Z.; Xu, H.; Gao, F.; Du, Y. Rapid synthesis of platinum-ruthenium bimetallic nanoparticles dispersed on carbon support as improved electrocatalysts for ethanol oxidation. *J. Coll. Interface Sci.* **2018**, *521*, 111–118. [CrossRef]

75. Marinkovic, N.S.; Li, M.; Adzic, R.R. Pt-based catalysts for electrochemical oxidation of ethanol. *Top. Curr. Chem.* **2019**, *377*, 11. [CrossRef]

76. Bai, J.; Liu, D.; Yang, J.; Chen, Y. Nanocatalysts for electrocatalytic oxidation of ethanol. *ChemSusChem* **2019**, *12*, 2117–2132. [CrossRef]

77. Tripkovic, A.V.; Lovic, J.D.; Popovic, K.D. Comparative study of ethanol oxidation at Pt-based nanoalloys and UDP-modified Pt nanoparticles. *J. Serb. Chem. Soc.* **2010**, *75*, 1559–1574. [CrossRef]

78. Li, M.; Kowal, A.; Sasaki, K.; Marinkovic, N.; Su, D.; Korach, E.; Liu, P.; Adzic, R.R. Ethanol oxidation on the ternary Pt-Rh-SnO$_2$/C electrocatalysts with varied Pt: Rh: Sn ratios. *Electrochim. Acta* **2010**, *55*, 4331–4338. [CrossRef]

79. Kowal, A.; Li, M.; Shao, M.; Sasaki, K.; Vukmirovic, M.; Zhang, J.; Marinkovic, N.; Liu, P.; Frenkel, A.; Adzic, R.R. Ternary Pt/Rh/SnO$_2$ electrocatalysts for oxidizing ethanol to CO$_2$. *Nat. Mater.* **2009**, *8*, 325–330. [CrossRef] [PubMed]

80. Kutz, R.B.; Braunschweig, B.; Mukherjee, P.; Behrens, R.L.; Dlott, D.D.; Wieckowski, A. Reaction pathways of ethanol electrooxidation on polycrystalline platinum catalysts in acidic electrolytes. *J. Catal.* **2011**, *278*, 181–188. [CrossRef]

81. Santasalo-Aarnio, A.; Tuomi, S.; Jalkanen, K.; Kontturi, K.; Kallio, T. The correlation of electrochemical and fuel cell results for alcohol oxidation in acidic and alkaline media. *Electrochim. Acta* **2013**, *87*, 730–738. [CrossRef]

82. Ma, L.; He, H.; Hsu, A.; Chen, R. PdRu/C catalysts for ethanol oxidation in anion-exchange membrane direct ethanol fuel cells. *J. Power Sources* **2013**, *241*, 696–702. [CrossRef]

83. Zhou, Z.Y.; Wang, Q.; Lin, J.L.; Tian, N.; Sun, S.G. In situ FTIR spectroscopic studies of electrooxidation of ethanol on Pd electrode in alkaline media. *Electrochim. Acta* **2010**, *55*, 7995–7999. [CrossRef]

84. Lai, S.C.S.; Koper, M.T.M. Ethanol electro-oxidation on platinum in alkaline media. *Phys. Chem. Chem. Phys.* **2009**, *11*, 10446–10456. [CrossRef]

85. García, G.; Koper, M.T.M. Stripping voltammetry of carbon monoxide oxidation on stepped platinum single-crystal electrodes in alkaline solution. *Phys. Chem. Chem. Phys.* **2008**, *10*, 3802–3811. [CrossRef]

86. Kutz, R.B.; Braunschweig, B.; Mukherjee, P.; Dlott, D.D.; Wieckowski, A. Study of ethanol electrooxidation in alkaline electrolytes with isotope labels and sum-frequency generation. *J. Phys. Chem. Lett.* **2011**, *2*, 2236–2240. [CrossRef]

87. Almeida, T.S.; van Wassen, R.R.; van Dover, R.B.; de Andrade, A.R.; Abruña, H.D. Combinatorial PtSnM (M = Fe, Ni, Ru and Pd) nanoparticle catalyst library toward ethanol electrooxidation. *J. Power Sources* **2015**, *284*, 623–630. [CrossRef]

88. Zhu WKe, J.; Wang, S.-B.; Ren, J.; Wang, H.-H.; Zhou, Z.-Y.; Si, R.; Zhang, Y.-W.; Yan, C.-H. Shaping single-crystalline trimetallic Pt-Pd-Rh nanocrystals toward high efficiency C-C splitting of ethanol in conversion to CO_2. *ACS Catal.* **2015**, *5*, 1995–2008.

89. Maillard, F.; Dubau, L.; Durst, J.; Chatenet, M.; André, J.; Rossinot, E. Durability of Pt_3Co/C nanoparticles in a proton-exchange membrane fuel cell: Direct evidence of bulk Co segregation to the surface. *Electrochem. Commun.* **2010**, *12*, 1161–1164. [CrossRef]

90. Dubau, L.; Maillard, F.; Chatenet, M.; Guetaz, L.; André, J.; Rossinot, E. Durability of Pt_3Co/C cathodes in a 16 cell PEMFC stack: Macro/microstructural changes and degradation mechanisms. *J. Electrochem. Soc.* **2010**, *157*, B1887–B1895. [CrossRef]

91. Pourbaix, M. *Atlas of Electrochemical Equilibria in Aqueous Solutions*, 2nd ed.; Pergamon Press: Brussels, Belgium, 1974.

92. Vej-Hansen, U.G.; Rossmeisl, J.; Stephens, I.E.L.; Schiotz, J. Correlation between diffusion barriers and alloying energy in binary alloys. *Phys. Chem. Chem. Phys.* **2016**, *18*, 3302–3307. [CrossRef] [PubMed]

93. Greeley, J.; Stephens, I.E.L.; Bondarenko, A.S.; Johansson, T.P.; Hansen, H.A.; Jaramillo, T.F.; Rossmeisl, J.; Chorkendorff, I.; Norskof, J.K. Alloys of platinum and early transition metals as oxygen reduction electrocatalysts. *Nat. Chem.* **2009**, *1*, 552–556. [CrossRef] [PubMed]

94. Stephens, I.E.L.; Bondarenko, A.S.; Gronbjerg, U.; Rossmeisl, J.; Chorkendorff, I. Understanding the electrocatalysis of oxygen reduction on platinum and its alloys. *Energy Environ. Sci.* **2012**, *5*, 6744–6762. [CrossRef]

95. Stephens, I.E.L.; Bondarenko, A.S.; Bech, L.; Chorkendorff, I. Oxygen electroreduction activity and X-ray photoelectron spectroscopy of platinum and early transition metal alloys. *ChemCatChem* **2012**, *4*, 341–349. [CrossRef]

96. Escudero-Escribano, M.; Verdaguer-Casadevall, A.; Malacrida, P.; Gronbjerg, U.; Knudsen, B.P.; Jepsen, A.K.; Rossmeisl, J.; Stephens, I.E.L.; Chorkendorff, I. Pt_5Gd as a highly active and stable catalyst for oxygen electroreduction. *J. Am. Chem. Soc.* **2012**, *134*, 16476–16479. [CrossRef]

97. Escudero-Escribano, M.; Malacrida, P.; Hansen, M.H.; Vej-Hansen, U.G.; Velasquez-Palenzuela, A.; Tripkov, V.; Schiotz, J.; Rossmeisl, J.; Stephens, I.E.L.; Chorkendorff, I. Tuning the activity of Pt alloy electrocatalysts by means of the lanthanide contraction. *Science* **2016**, *352*, 73–76. [CrossRef]

98. Malacrida, P.; Escudero-Escribano, M.; Verdaguer-Casadevall, A.; Stephens, I.E.L.; Chorkendorff, I. Enhanced activity and stability of Pt-La and Pt-Ce alloys for oxygen electroreduction: The elucidation of the active surface phase. *J. Mater. Chem. A* **2014**, *2*, 4234–4243. [CrossRef]

99. Hultgren, R. *Selected Values of the Thermodynamic Properties of Binary Alloys*; American Society for Metals: Metals Park, OH, USA, 1973.

100. Kleykamp, H. Thermodynamics of the systems of the platinum metals with other transition metals: I. Integral data. *J. Nucl. Mater.* **1993**, *201*, 193–217. [CrossRef]

101. Walker, R.; Darby, J. Thermodynamic properties of solid nickel-platinum alloys. *Acta Metall.* **1970**, *18*, 1261–1266. [CrossRef]

102. Pretorius, R.; Morais, T.; Theron, C. Thin film compound phase formation sequence: An effective heat of formation model. *Mater. Sci. Rep.* **1993**, *10*, 1–83. [CrossRef]

103. Jacob, K.; Waseda, Y. Gibbs energies of formation of rare earth MPt_5 compounds. *Thermochim. Acta* **1990**, *165*, 223–233. [CrossRef]

104. Kitchin, J.R.; Norskov, J.K.; Barteau, M.A.; Chem, J.G. Modification of the surface electronic and chemical properties of Pt(111) by subsurface 3d transition metals. *J. Chem. Phys.* **2004**, *120*, 10240–10246. [CrossRef]

105. Strasser, P.; Koh, S.; Anniyev, T.; Greeley, J.; More, K.; Yu, C.; Liu, Z.; Kaya, S.; Nordlund, D.; Ogasawara, H.; et al. Laltice-strain control of the activity in dealloyed core-shell fuel cell catalysts. *Nat. Chem.* **2010**, *2*, 454–460. [CrossRef] [PubMed]

106. Erlebacher, J.; Marguis, D. Mechanism of hollow nanoparticle formation due to shape fluctuations. *Phys. Rev. Lett.* **2014**, *112*, 155505. [CrossRef]

107. Han, B.; Carlton, C.E.; Suntivich, J.; Xu, Z.; Shao-Horn, Y. Oxygen reduction activity and stability trends of bimetallic $Pt_{0.5} M_{0.5}$ nanoparticle in acid. *J. Phys. Chem. C* **2015**, *119*, 3971–3978. [CrossRef]

108. Johansson, T.P.; Ulrikkeholm, E.T.; Hernandez-Fernandez, P.; Escudero-Escribano, M.; Malacrida, P.; Stephens, I.E.L.; Chorkendorff, I. Towards the elucidation of the high oxygen electroreduction activity of Pt_xY: Surface science and electrochemical studies of Y/Pt (111). *Phys. Chem. Chem. Phys.* **2014**, *16*, 13718–13725. [CrossRef]

109. Ulrikkeholm, E.T.; Pedersen, A.F.; Vej-Hansen, U.G.; Escudero-Escribano, M.; Stephens, I.E.; Friebel, D.; Mehta, A.; Schiotz, J.; Feidenhansl, R.K.; Nilsson, A.; et al. Pt_xGd alloy formation on Pt (111): Preparation and structural characterization. *Surf. Sci.* **2016**, *652*, 114–122. [CrossRef]

110. Pedersen, A.F.; Ulrikkeholm, E.T.; Escudero-Escribano, M.; Johansson, T.P.; Malacrida, P.; Pedersen, C.M.; Hansen, M.H.; Jensen, K.D.; Rossmeisl, J.; Friebel, D.; et al. Probing the nanoscale structure of the catalytically active overlayer on Pt alloys with rare earths. *Nano Energy* **2016**, *29*, 249–260. [CrossRef]

111. Paulo, M.J.; Venancio, R.H.D.; Freitas, R.G.; Pereira, E.C.; Tavares, A.C. Investigation of the electrocatalytic activity for ethanol oxidation of Pt nanoparticles modified with small amount (5 wt%) of CeO_2. *J. Electroanal. Chem.* **2019**, *840*, 367–375. [CrossRef]

112. Jacob, J.; Corradini, P.; Antolini, E.; Santos, N.A.; Perez, J. Electro-oxidation of ethanol on ternary Pt-Sn-Ce/C catalysts. *Appl. Catal. B Environ.* **2015**, *165*, 176–184. [CrossRef]

113. Wang, Q.; Liu, Z.; An, S.; Wang, R.; Wang, Y.; Xu, T. Effect of CeO_2–ZrO_2 on Pt/C electrocatalysts for alcohols oxidation. *J. Rare Earths* **2016**, *34*, 276–282. [CrossRef]

114. Corddacho-Garcia, J.; Betancourt, L.E.; Velez, C.A.; Senanayake, S.D.; Stacchiola, D.; Sasaki, K.; Guinel, M.J.-F.; Zhou, Y.; Cheung, C.L.; Cabrera, C.R. Cerium oxide as a promoter for the electrooxidation reaction of ethanol: In situ XAFS characterization of the Pt nanoparticles supported on CeO_2 nanoparticles and nanorods. *Phys. Chem. Chem. Phys.* **2015**, *17*, 32251–32256. [CrossRef] [PubMed]

115. Xiang, S.; Wang, L.; Huang, C.-C.; Fan, Y.-Z.; Tang, H.-G.; Wei, L.; Sun, S.-G. Concave cubic PtLa alloy nanocrystals with high-index facets: Controllable synthesis in deep eutectic solvents and their superior electrocatalytic properties for ethanol oxidation. *J. Power Sources* **2018**, *399*, 422–428. [CrossRef]

116. Corradini, P.G.; Santos, N.A.; Perez, J. Pt-Sn-Eu/C catalysts: Application of rare earth metals as anodes in direct ethanol fuel cells. *Fuel Cells* **2018**, *18*, 73–81. [CrossRef]

117. Corradini, P.G.; Antolini, E.; Perez, J. Electrooxidation of ethanol on ternary non-alloyed Pt-Sn-Pr/C catalysts. *J. Power Sources* **2015**, *275*, 377–383. [CrossRef]

118. Corradini, P.G.; Antolini, E.; Perez, J. Activity, short-term stability (poisoning tolerance) and durability of carbon supported Pt-Pr catalysts for ethanol oxidation. *J. Power Sources* **2014**, *251*, 402–410. [CrossRef]

119. Ma, Y.; Du, Y.; Ye, W.; Su, B.; Yang, M.; Wang, C. Electrocatalytic oxidation of ethanol on platinum electrode decorated with Nd-Fe-Mo hybrid-metallic cyano-bridged mixing coordination polymer in weak acidic medium. *Int. J. Electrochem. Sci.* **2012**, *7*, 2654–2679.

120. Song, S.; Tsiakaras, P. Recent progress in direct ethanol proton exchange membrane fuel cells (DE-PEMFCs). *Appl. Catal. B Environ.* **2006**, *63*, 187–193. [CrossRef]

121. Abdullah, S.; Kamarudin, S.K.; Hasran, U.A.; Masdar, M.S.; Daud, W.R.W. Development of a conceptual design model of a direct ethanol fuel cell (DEFC). *Int. J. Hydrog. Energy* **2015**, *40*, 11943–11948. [CrossRef]

122. Duan, J.J.; Feng, J.J.; Zhang, L.; Yuan, J.; Zhang, Q.L.; Wang, A.J. Facile one-pot aqueous fabrication of interconnected ultrathin PtPbPd nanowires as advanced electrocatalysts for ethanol oxidation and oxygen reduction reactions. *Int. J. Hydrog. Energy* **2019**, *44*, 27455–27464. [CrossRef]

123. Carrera-Cerritos, R.; Fuentes-Ramírez, R.; Cuevas-Muñiz, F.M.; Ledesma-García, J.; Arriaga, L.G. Performance and stability of Pd nanostructures in an alkaline direct ethanol fuel cell. *J. Power Sources* **2014**, *269*, 370–378. [CrossRef]

124. Cardoso, D.S.P.; Santos, D.M.F.; Šljukić, B.; Sequeira, C.A.C.; Macciò, D.; Saccone, A. Platinum-rare earth cathodes for direct borohydride-peroxide fuel cells. *J. Power Sources* **2016**, *307*, 251–258. [CrossRef]

125. Santos, D.M.F.; Saturnino, P.G.; Macciò, D.; Saccone, A.; Sequeira, C.A.C. Platinum rare-earth intermetallic alloys as anode electrocatalysts for borohydride oxidation. *Catal. Today* **2011**, *170*, 134–140. [CrossRef]

126. Šljukić, B.; Milikić, J.; Santos, D.M.F.; Sequeira, C.A.C.; Macciò, D.; Saccone, A. Electrocatalytic performance of Pt-Dy alloys for direct borohydride fuel cells. *J. Power Sources* **2014**, *272*, 335–343. [CrossRef]

127. Santos, D.M.F.; Šljukić, B.; Sequeira, C.A.C.; Macciò, D.; Saccone, A.; Figueiredo, J.L. Electrocatalytic approach for the efficiency increase of electrolytic hydrogen production: Proof-of-concept using Pt-Dy. *Energy* **2013**, *50*, 486–492. [CrossRef]

128. Santos, D.M.F.; Sequeira, C.A.C.; Macciò, D.; Saccone, A.; Figueiredo, J.L. Platinum rare earth electrodes for hydrogen evolution in alkaline water electrolysis. *Int. J. Hydrog. Energy* **2013**, *38*, 3137–3145. [CrossRef]

129. Moulder, J.F.; Stickle, W.F.; Sobol, P.E.; Bomben, K.D. *Handbook of X-ray Photoelectron Spectroscopy*, 2nd ed.; PHI: Eden Prairie, MN, USA, 1992.

130. Xie, S.W.; Chen, S.; Liu, Z.Q.; Xu, C.W. Comparison of alcohol electrooxidation on Pt and Pd electrodes in alkaline medium. *Int. J. Electrochem. Soc.* **2011**, *6*, 882–888.

131. Brownson, D.A.C.; Banks, C.E. Interpreting electrochemistry. In *The Handbook of Graphene Electrochemistry*; Springer: London, UK, 2014; pp. 23–77.

132. Bard, A.J.; Faulkner, L.R. Potential sweep methods. In *Electrochemical Methods: Fundamentals and Applications*, 2nd ed.; John Wiley & Sons: New York, NY, USA, 2001; pp. 226–260.

133. Denuault, G.; Mirkin, M.V.; Bard, A.J. Direct determination of diffusion coefficients by chronoamperometry at microdisk electrodes. *J. Electroanal. Chem.* **1991**, *308*, 27–38. [CrossRef]

134. Wang, K.; Lu, J.; Zhuang, L. Direct determination of diffusion coefficient for borohydride anions in alkaline solutions using chronoamperometry with spherical Au electrodes. *J. Electroanal. Chem.* **2005**, *585*, 191–196. [CrossRef]